Engineering Analysis with Boundary Elements 36 (2012) 1301–1310

Contents lists available at SciVerse ScienceDirect

Engineering Analysis with Boundary Elements

journal homepage: www.elsevier.com/locate/enganabound

A dual reciprocity boundary face method for 3D non-homogeneous elasticity problems

Fenglin Zhou [a], Jianming Zhang [a,b,*], Xiaomin Sheng [a], Guangyao Li [a]

[a] State Key Laboratory of Advanced Design and Manufacturing for Vehicle Body, College of Mechanical and Vehicle Engineering, Hunan University, Changsha 410082, China
[b] State Key Laboratory of Structural Analysis for Industrial Equipment, Dalian University of Technology, Dalian 116023, China

ARTICLE INFO

Article history:
Received 2 December 2011
Accepted 4 March 2012

Keywords:
Boundary face method
Dual reciprocity method
Radial basis function
Non-homogeneous elasticity
Thin shell-like structure

ABSTRACT

The boundary face method is coupled with the dual reciprocity method (DRM) to solve non-homogeneous elasticity problems. We will analyze thin structures based on 3D solid elastic theory rather than the shell theory as in the finite element method (FEM). To circumvent the ill-conditioning problem that occurs in the radial basis function (RBF) approximation in thin structures, a special variation scheme for determining the RBF parameters is proposed. In addition, a new exponential RBF is used which has significantly improved the stability of the RBF, and its particular solution to the elasticity problem is derived for the first time. Comparisons of our method with the traditional DRM, the boundary element method (BEM) and the FEM have been made. Numerical examples have demonstrated that our method outperforms the BEM and FEM with respect to stability, accuracy and efficiency, especially when the structure in question has features of small size, such as thin shells.

1. Introduction

The boundary element method (BEM) is an efficient alternative numerical technique for solving engineering problems, such as Laplace equation, Navier's equation, Helmholtz equation and linear diffusion-reaction equation [1–4]. In the BEM, partial differential equations (PDEs) are converted to an equivalent boundary integral equation (BIE) by Green's theorem and a fundamental solution. Thus, only boundary discretization can lead to an accurate result together with a high rate of convergence. This is the main advantage over the classic domain methods such as finite element method (FEM) and finite difference method (FDM).

Very recently, Zhang et al. have proposed the boundary face method (BFM) based on BEM to make direct use of the boundary representation (B-rep) data structure that is used in most CAD packages for geometry modeling [5]. Similar with the widely studied isogeometric analysis [6–8], the BFM has potential to interact with the CAD packages seamlessly. Nevertheless, the BFM is a bit different from the isogeometric analysis. The isogeometric analysis applies the Non-Uniform Rational B-Splines (NURBS) as the approximation function for both of the geometric quantities and physical variables [6]. In the BFM, both boundary integration and variable approximation are performed in the parametric space as in the hybrid boundary node method (HdBNM) [9–11]. The integrand quantities are calculated directly from boundary faces rather than elements as in the standard BEM, thus geometric errors can be avoided. When the BFM is implemented using shape functions from the Moving Least Squares [5], it becomes a meshless method, and the BFM can be considered as a new implementation of the boundary node method (BNM) [12–13]. Recently, Qin and Zhang have implemented the BFM using finite elements defined in the parametric space of boundary faces [14], which can be considered as a new implementation of the BEM.

Nevertheless, when dealing with non-homogeneous, non-linear problems and those to which fundamental solutions are unavailable, the BEM and the BFM become less attractive since domain integrals that remain in the BIE should be calculated. To avoid the domain integrals, several methods have been proposed including the radial integration method (RIM) [15] and the dual reciprocity method (DRM) [16]. In both methods, a number of points inside the domain should be applied. In the RIM, these points are applied to approximate the domain integral kernel appeared in the integral equation. In the DRM, the non-homogeneous term of the PDE is approximated by a series of simple functions, and the domain integral of this non-homogeneous term is transformed to the boundary integrals by employing particular solutions of considered problem. It is worth noting that no meshes are required for variable approximation inside the considered domain. In this work, the DRM is combined with the BFM to solve the elasticity problem with body forces for the first time. We call the combined method the dual reciprocity boundary face

* Corresponding author. Tel.: +86 0731 888 23061.
E-mail addresses: zhangjm@hnu.edu.cn, zhangjianm@gmail.com (J. Zhang).

0955-7997/$ - see front matter © 2012 Elsevier Ltd. All rights reserved.
http://dx.doi.org/10.1016/j.enganabound.2012.03.009

method (DRBFM). Since the accuracy and the stability of the solution depend largely on the approximation, the choice of the approximating functions is usually of crucial importance in the DRM implementation. The most widely used approximating functions are radial basis functions (RBFs).

The RBF interpolation is efficient in scattered data approximation. The ill-conditioned matrix generated by RBF interpolation, however, limits its application in the large scale problems and problems on thin structures. In order to circumvent the ill conditioning problem appearing in the RBF interpolation, many methods had been proposed such as the compact support RBF, the multilevel method, the domain decomposition method, variable shaped RBF and so on [17]. This paper uses variable shaped RBF to circumvent the ill-conditioning problem.

In the variable shaped RBF method, the choice of the variation scheme of the shape parameter is of great importance to the accuracy and the stability of the interpolation. Sarra and Sturgill [18] had verified a random variation scheme and Li, Zhu and Zhang [19] had implemented a linear scheme successfully. In those papers, the variable shaped RBF was implemented to improve the accuracy of the interpolation rather than the stability of the interpolation. In engineering problems, however, the stability of the method is usually much more important, since the analytical solutions for these problems are usually unavailable. With more emphasis on the stability of the interpolation, Zhou et. al. [20] had proposed several variation schemes for Multiquadric RBF and applied them to solve nonhomogeneous potential problems.

This paper extends the DRBFM to solve the nonhomogeneous elasticity problems. In this implementation, the variable shaped exponential RBF is applied. A special variation scheme for problems on thin structures is proposed. Using the method of Papkovich potentials [21], the particular solution is deduced. The limitation case of the particular solution has also been considered. To the author's knowledge, the particular solution of this exponential RBF for Navier equation is presented for the first time.

As numerical examples, four non-homogeneous elasticity problems on different structures are analyzed. Comparison study between the conventional DRBEM and the DRBFM are made in the first example. By equipping with the proposed variation scheme, the stability of the DRBFM for the problem on thin structure is illustrated in the second example. To demonstrate the accuracy of the stress calculated by our method, a non-homogeneous elasticity problem on an elbow shaped pipe is solved in the third example. In the last example, a real-world structure with a small feature is analyzed. Small features are usually omitted in the FEM analysis, as the degree of freedoms increases considerably if these small features are considered in the grid model. The geometrical simplification often results in very poor accuracy of stress at the small features. Nevertheless, the local stresses are more concerned by design engineers. For thin shell-like structures, shell elements, which introduce additional strain assumptions, are usually employed in the FEM. Solid elements with proper aspect ratios should be used when high accuracy is demanded. This will, however, result in large FEM models, and it may be difficult to generate the FEM mesh for thin shell-like structures if the geometry is complicated. In contrast, the analysis by BIE based methods including BEM [22–25] and BFM can be directly performed without any additional geometric assumptions. In BFM, thin shell-like structures and structures with feature of small size can be analyzed without any geometric simplification or assumption. The result in last example has showed the attractive feature of the proposed approach.

This paper is organized as follows. In Section 2, the DRBFM for non-homogeneous elasticity problems is described. Section 3 presents the exponential RBF and variation schemes followed by the derivation of the particular solution in Section 4. Four numerical examples are presented in Section 5. This paper ends with conclusions and future work in Section 6.

2. The dual reciprocity boundary face method for elasticity

This section gives a short description of the DRM. For more details about this method, readers are suggested to consult [26].

We start from a boundary value problem in nonhomogeneous elasticity theory:

$$\begin{cases} Gu_{i,jj}+\frac{G}{1-2\nu}u_{j,ji}+b_i=0 & X\in\Omega \\ u_i=\overline{u}_i & X\in\Gamma_1 \\ p_i=\sigma_{ij}n_j=\overline{p}_i & X\in\Gamma_2 \end{cases} \tag{1}$$

where the domain Ω is enclosed by $\Gamma=\Gamma_1\cup\Gamma_2$, G, ν stand for the shear module and Poisson rate of the material. $b_i=b_i(X)$ is the distribution of the body force, $\overline{u}_i$ and $\overline{p}_i$ denote for the prescribed displacements and tractions on the essential boundary Γ_1 and on the nature boundary Γ_2, respectively. σ_{ij} is the stress component and n is the outward normal direction to the boundary Γ, with components n_i, $i=1,2,3$.

In the DRM, the body force term is approximated by a series of RBFs.

$$b_i\approx\sum_{k=1}^{N+L}\alpha_k^i\varphi_k \tag{2}$$

where N and L are the number of boundary points and inner points, respectively. $\boldsymbol{\alpha}^{\mathbf{i}}=\{\alpha_1^i,\alpha_2^i,\cdots,\alpha_{N+L}^i\}^T$ is the coefficient vector, which can be determined by the following equation:

$$F\boldsymbol{\alpha}^i=\mathbf{b}_i \tag{3}$$

in which F is the interpolation matrix of order $N+L$, and the entry of vector $\boldsymbol{b}_i$ are values of the interpolated function at each point. The particular solution $\tilde{u}_{mj}^k$ satisfies the governing equation:

$$G\tilde{u}_{mj,ll}^k+\frac{G}{1-2\nu}\tilde{u}_{lj,lm}^k=\delta_{mj}\varphi_k \tag{4}$$

Substituting Eq. (4) into Eq. (2), and then into the governing equation, we have

$$Gu_{i,jj}+\frac{G}{1-2\nu}u_{j,ji}=\sum_{k=1}^{N+L}\alpha_k^i\left(G\tilde{u}_{mj,ll}^k+\frac{G}{1-2\nu}\tilde{u}_{lj,lm}^k\right) \tag{5}$$

The same procedure for developing the BEM for the homogeneous Navier's equation is applied on both part of Eq. (5), producing the boundary integral equation (BIE):

$$\begin{aligned} &c_{lj}^iu_j^i+\int_\Gamma p_{lj}^*u_j\mathrm{d}\Gamma-\int_\Gamma u_{lj}^*p_j\mathrm{d}\Gamma \\ &\quad=\sum_{k=1}^{N+L}\alpha_k^m(c_{lj}^i\tilde{u}_{mj}^{ik}+\int_\Gamma p_{lj}^*\tilde{u}_{mj}^k\mathrm{d}\Gamma-\int_\Gamma u_{lj}^*\tilde{p}_{mj}^k\mathrm{d}\Gamma) \end{aligned} \tag{6}$$

where u_{lj}^*,q_{lj}^* are the fundamental solution to the Navier's equation and its corresponding traction, respectively.

$$c_{lj}^i=\frac{\delta_{lj}}{2} \tag{7}$$

is a constant if Γ is a smooth boundary.

Instead of the BEM, the BFM is applied to solve this BIE in this implementation. In the conventional BEM, the geometry coordinates are approximated through the standard element, thus geometric errors are inevitably produced. In the BFM, both the integration over the boundary and the variable approximation are performed in the parametric space. The integrand quantities such as the coordinates of Gauss integration points, Jacobian and out normal are calculated directly from the faces, which are represented in parametric form,

rather than from standard elements. Thus geometric error can be avoided. For more details about BFM, readers are suggested to [5]. After the boundary discretization and the boundary variable approximation, we have the discretized BIE:

$$c_{ij}^{i}u_j^i+\sum_{t=1}^{N}\int_{\Gamma_t}p_{ij}^{*}(s,x_i)\sum_{n=1}^{N}N_n(s)u_{jn}\mathrm{d}\Gamma(s)-\sum_{t=1}^{N}\int_{\Gamma_t}u_{ij}^{*}(s,x_i)\sum_{n=1}^{N}N_n(s)p_{jn}\mathrm{d}\Gamma(s)$$
$$=\sum_{k=1}^{N+L}\alpha_k^m\left(c_{ij}^{i}\tilde{u}_{mj}^{ik}+\sum_{t=1}^{N}\int_{\Gamma_t}p_{ij}^{*}(s,x_i)\sum_{n=1}^{N}N_n(s)\tilde{u}_{mnj}^{k}\mathrm{d}\Gamma(s)-\sum_{t=1}^{N}\int_{\Gamma_t}u_{ij}^{*}(s,x_i)\sum_{n=1}^{N}N_n(s)\tilde{p}_{mnj}^{k}\mathrm{d}\Gamma(s)\right) \tag{8}$$

where

$$u_{jn}=u_j(x_n) \tag{9}$$

and

$$p_{jn}=p_j(x_n) \tag{10}$$

The physical variable approximation on the boundary is performed in the parametric space. It is of the form:

$$u_j(x,y,z)=u_j(u,v)=u_j(\xi,\eta)=\sum_{n=1}^{N}N_n(\xi,\eta)u_{jn}$$
$$q_j(x,y,z)=u_j(u,v)=u_j(\xi,\eta)=\sum_{n=1}^{N}N_n(\xi,\eta)q_{jn} \tag{11}$$

where (u,v) is the parametric coordinate of (x,y,z) on the surface, and (ξ,η) is the corresponding normalized parametric coordinate.

The matrix form of Eq. (6) is

$$H\mathbf{u}-G\mathbf{p}=(H\hat{U}-G\hat{P})\boldsymbol{\alpha} \tag{12}$$

in which

$$\hat{U}=\begin{bmatrix}\hat{\mathbf{u}}_{11}&\hat{\mathbf{u}}_{12}&\hat{\mathbf{u}}_{13}\\ \hat{\mathbf{u}}_{21}&\hat{\mathbf{u}}_{22}&\hat{\mathbf{u}}_{23}\\ \hat{\mathbf{u}}_{31}&\hat{\mathbf{u}}_{32}&\hat{\mathbf{u}}_{33}\end{bmatrix},\quad \hat{\mathbf{u}}_{mk}^{ij}=\tilde{u}_{mk}(x_i,x_j) \tag{13}$$

$$\hat{P}_{ij}=\begin{bmatrix}\hat{\mathbf{p}}_{11}&\hat{\mathbf{p}}_{12}&\hat{\mathbf{p}}_{13}\\ \hat{\mathbf{p}}_{21}&\hat{\mathbf{p}}_{22}&\hat{\mathbf{p}}_{23}\\ \hat{\mathbf{p}}_{31}&\hat{\mathbf{p}}_{32}&\hat{\mathbf{p}}_{33}\end{bmatrix},\quad \hat{\mathbf{p}}_{mk}^{ij}=\tilde{p}_{mk}(x_i,x_j) \tag{14}$$

$$\boldsymbol{\alpha}=\begin{bmatrix}\boldsymbol{\alpha}^1\\ \boldsymbol{\alpha}^2\\ \boldsymbol{\alpha}^3\end{bmatrix} \tag{15}$$

$$H=\begin{bmatrix}\mathbf{p}_{11}^{*}&\mathbf{p}_{12}^{*}&\mathbf{p}_{13}^{*}\\ \mathbf{p}_{21}^{*}&\mathbf{p}_{22}^{*}&\mathbf{p}_{23}^{*}\\ \mathbf{p}_{31}^{*}&\mathbf{p}_{32}^{*}&\mathbf{p}_{33}^{*}\end{bmatrix} \tag{16}$$

$$\mathbf{p}_{mk}^{*ij}=\sum_{t=1}^{N}\int_{\Gamma_t}p_{mk}^{*}(x,x_i)N_j(x)\mathrm{d}\Gamma(x) \tag{17}$$

$$G=\begin{bmatrix}\mathbf{u}_{11}^{*}&\mathbf{u}_{12}^{*}&\mathbf{u}_{13}^{*}\\ \mathbf{u}_{21}^{*}&\mathbf{u}_{22}^{*}&\mathbf{u}_{23}^{*}\\ \mathbf{u}_{31}^{*}&\mathbf{u}_{32}^{*}&\mathbf{u}_{33}^{*}\end{bmatrix} \tag{18}$$

$$\mathbf{u}_{mk}^{*ij}=\sum_{t=1}^{N}\int_{\Gamma_t}u_{mk}^{*}(x,x_i)N_j(x)\mathrm{d}\Gamma(x) \tag{19}$$

$$\mathbf{u}=\begin{bmatrix}\mathbf{u}^1\\ \mathbf{u}^2\\ \mathbf{u}^3\end{bmatrix},\quad \mathbf{p}=\begin{bmatrix}\mathbf{p}^1\\ \mathbf{p}^2\\ \mathbf{p}^3\end{bmatrix},\quad \mathbf{u}_j^i=u_i(x_j),\quad \mathbf{p}_j^i=p_i(x_j) \tag{20}$$

After Eq. (12) is solved, the displacement at any internal location can be calculated from the equation:

$$u_l(x)+\sum_{t=1}^{N}\int_{\Gamma_t}p_{ij}^{*}(s,x)\sum_{n=1}^{N}N_n(s)u_{jn}\mathrm{d}\Gamma(s)-\sum_{t=1}^{N}\int_{\Gamma_t}u_{ij}^{*}(s,x)\sum_{n=1}^{N}N_n(s)p_{jn}\mathrm{d}\Gamma(s)$$
$$=\sum_{k=1}^{N+L}\alpha_k^m\left(\tilde{u}_{ml}^{k}(x)+\sum_{t=1}^{N}\int_{\Gamma_t}p_{ij}^{*}(s,x)\sum_{n=1}^{N}N_n(s)\tilde{u}_{mnj}^{k}\mathrm{d}\Gamma(s)-\sum_{t=1}^{N}\int_{\Gamma_t}u_{ij}^{*}(s,x)\sum_{n=1}^{N}N_n(s)\tilde{p}_{mnj}^{k}\mathrm{d}\Gamma(s)\right) \tag{21}$$

It worth noting that there are singular integrals appearing in the diagonal terms of the matrix (16) and (18). Singular integrals in matrix (16) were handled by a simple solution method introduced in [27]. Singular integrals in matrix (18) were calculated through a triangular transformation which was introduced by Zhang et. al. in [5].

The scheme for calculating nearly singular integral is of great importance to BIE based method to analyzed thin structure [22–25]. The scheme we applied in this paper is the subdivision scheme. The main idea of this scheme is employing more integral points to calculate the integral over the boundary patches near the source points. For more details, refer to [5].

3. The variable shaped exponential RBF and the variation schemes

The approximation function plays a key role in the DRM. In most cases, RBFs are chosen to be the approximation functions. In this paper, the exponential RBF is applied. It is of the form:

$$\varphi_i(r)=e^{-cr_i} \tag{22}$$

Although the positive definiteness of the interpolation matrix has not been guaranteed theoretically, accurate results can be obtained using this type of RBF. It is noted that the parameter c controls the shape of the interpolation function. To improve the accuracy of the interpolation, large value of this shape parameter is usually applied. Large value of the parameter, however, results in ill-conditioned interpolation matrix. In engineering problems, the stability of the method is usually much more important than the accuracy since the exact solutions are usually unavailable. To keep the stability of the interpolation, a variable shaped exponential RBF is applied in this work. The variable shaped exponential RBF is of the form

$$\varphi_i(r)=e^{-c_ir_i} \tag{23}$$

in which the shape parameter varies according to the interpolation center. The variation scheme for the parameter of the exponential RBF we suggest is:

$$c_i=\frac{a}{D_i} \tag{24}$$

D_i satisfies that there are 40–100 points in the ball, which is centered at x_i and whose radius is D_i. The constant

$$\ln 2\le a\le \ln 10 \tag{25}$$

is suggested. The determination of the constant will be discussed as follows.

In Fig. 1, 40–100 neighbor points are located in the interval $(0,D_i)$. To guarantee the accuracy of the interpolation, the value of e^{-a} should be as large as possible. In the other hand, small value of e^{-a} should be applied to keep the interpolation stable. In order to balance the two contradictive factors

$$\tfrac{1}{10}<=e^{-(a/D_i)D_i}=e^{-a}<=\tfrac{1}{2} \tag{26}$$

is suggested. We have implemented numerical experiments with the parameter provided by this formula for thousands of times and we found this formula is effective.

In problems on thin structures, some boundary nodes are usually very close. This phenomenon can be illustrated in Fig. 2.

The distance matrix for the points in Fig. 2 is

$$\begin{bmatrix} 0 & 0.001 & 1 \\ 0.001 & 0 & 1 \\ 1 & 1 & 0 \end{bmatrix} \tag{27}$$

Assuming $c=1$, the corresponding interpolation matrix is

$$\begin{bmatrix} 1 & \frac{1}{e^{0.001}} & \frac{1}{e} \\ \frac{1}{e^{0.001}} & 1 & \frac{1}{e} \\ \frac{1}{e} & \frac{1}{e} & 1 \end{bmatrix} \tag{28}$$

The cosine of the angle between the first row vector and the second row vector is 0.99999953. Obviously, the first row and second row of the interpolation matrix are highly linear dependent. This will cause serious problems in interpolation stability.

In order to make the first row and the second row more linear independent, the parameter of the RBF which are centered at two close points should be as large as possible. The special variation scheme for problems on thin structures we propose is:

$$\begin{cases} c_i = \frac{a}{d_i} & x_i \in \Gamma \\ c_i = \frac{a}{D_i} & x_i \in \Omega \end{cases} \tag{29}$$

in which d_i is the distance between the i*th* interpolation point and its nearest points. Applying this variation scheme with

$$a = \ln 3 \tag{30}$$

as suggested before, the interpolation matrix becomes

$$\begin{bmatrix} 1 & \frac{1}{3} & \frac{1}{3^{1000}} \\ \frac{1}{3} & 1 & \frac{1}{3^{1000}} \\ \frac{1}{3} & \frac{1}{3} & 1 \end{bmatrix} \tag{31}$$

The cosine of the angle between the first row vector and the second row vector becomes 0.6. The condition of the matrix becomes much better. It should be noted that, in order to guarantee the accuracy of the interpolation, one additional domain point between two boundary nodes should be applied.

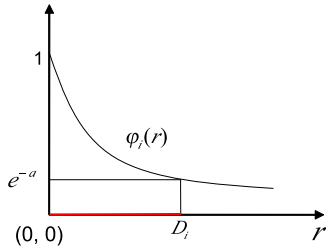

Fig. 1. Evaluation of constant *a*.

4. Particular solutions to Navier equation

In the DRM implementation, the analytical particular solution of the RBF is necessary. Many methods had been proposed for deducing the particular solution to Navier equation such as Galerkin vector method and method using Papkovich potentials. This paper applies the Popkovich potential to derive the particular solution. For more details about the procedure, refer to [21].

The Navier equation can be represented by the matrix form:

$$G\mathbf{I}\Delta + (\lambda+G)\nabla\nabla(\mathbf{\Psi}) = \varphi(r)\mathbf{I} \tag{32}$$

in which G,λ are the Lame constant of the material, $\mathbf{I}$ stands for the identity matrix of 3 orders and $\mathbf{\Psi}$ denotes for the particular displacement in matrix form. The particular displacements for this equation can be decomposed into the form:

$$\mathbf{\Psi} = \boldsymbol{\alpha}_1 \otimes \mathbf{e}_1 + \boldsymbol{\alpha}_2 \otimes \mathbf{e}_2 + \boldsymbol{\alpha}_3 \otimes \mathbf{e}_3 \tag{33}$$

where $\boldsymbol{\alpha}_i, \mathbf{e}_i$ are unknown coefficient vector and the unit vector along x_i axes. $\otimes$ denotes for the dyadic. Inserting Eq. (33) into Eq. (32), we obtain:

$$\sum_{k=1}^{3} [G\Delta\boldsymbol{\alpha}_k + (\lambda+G)\nabla\nabla\cdot\boldsymbol{\alpha}_k - \varphi(r)\mathbf{e}_k] \otimes \mathbf{e}_k = \mathbf{0} \tag{34}$$

that is

$$\Delta\boldsymbol{\alpha}_k + \frac{1}{1-2\nu}\nabla\nabla\cdot\boldsymbol{\alpha}_k - \frac{1}{G}\varphi(r)\mathbf{e}_k = \mathbf{0}, \quad k = 1,2,3 \tag{35}$$

The particular solution to Eq. (35) can be expressed by:

$$\boldsymbol{\alpha}_k = \mathbf{A}_k - \frac{1}{4(1-\nu)}\nabla(\mathbf{r}\cdot\mathbf{A}_k + \alpha_k), \quad k = 1,2,3 \tag{36}$$

where the vector $\boldsymbol{A}_k$ and scalar α_k satisfy the equation:

$$G\Delta\mathbf{A}_k = \varphi(r)\mathbf{e}_k \tag{37}$$

and

$$G\Delta\alpha_k = -\varphi(r)(\mathbf{r}\cdot\mathbf{e}_k) \tag{38}$$

the solutions to Eq. (37) and to Eq. (38) are, respectively:

$$G\mathbf{A}_k = \left[g(r) + \frac{c_1}{r}\right]\mathbf{e}_k + \frac{c_2}{r}(\mathbf{e}_1 + \mathbf{e}_2 + \mathbf{e}_3 - \mathbf{e}_k) \tag{39}$$

$$G\alpha_k = \left[q(r) + c_3 r + \frac{c_4}{r^2}\right](\mathbf{r}\cdot\mathbf{e}_k) \tag{40}$$

where c_1, c_2, c_3, c_4 is the integral constant. $g(r)$ and $q(r)$ satisfy the equations:

$$\frac{1}{r}\frac{\mathrm{d}}{\mathrm{d}r}\left(\frac{\mathrm{d}}{\mathrm{d}r}(rg(r))\right) = \varphi(r) \tag{41}$$

$$\frac{\mathrm{d}}{\mathrm{d}r}\left(\frac{1}{r^2}\frac{\mathrm{d}}{\mathrm{d}r}(r^2 q(r))\right) = -r\varphi(r) \tag{42}$$

Substitute Eq. (39) and Eq. (40) into Eq. (36), and then inserting into Eq. (33). We obtain the complete solution to Eq. (32)

$$\tilde{u}_{ij}(r) = p_1(r)\delta_{ij} + p_2(r)r_i r_j \tag{43}$$

in which

$$p_1(r) = \frac{3-4\nu}{4(1-\nu)G}g(r) - \frac{1}{4(1-\nu)G}\frac{q(r)}{r} \tag{44}$$

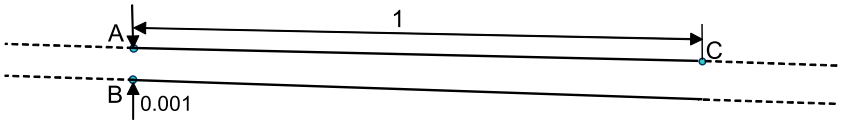

Fig. 2. Nodes on a thin shell.

$$p_2(r)=\frac{-1}{4(1-\nu)G}\left(\frac{g'(r)}{r}+\frac{q'(r)}{r^2}-\frac{q(r)}{r^3}\right) \tag{45}$$

In this paper, the exponential RBF is applied. The corresponding $g(r)$ and $q(r)$ are

$$g(r)=\frac{(2+rc)e^{-cr}-2}{c^3r} \tag{46}$$

$$q(r)=-\left(\frac{r}{c^2}+\frac{4}{c^3}+\frac{8}{c^4r}+\frac{8}{c^5r^2}\right)e^{-cr}+\frac{8}{c^5r^2} \tag{47}$$

It is worth noting that proper evaluation of the integral constants is important to keep

$$g(r)\in C^1(\Omega) \tag{48}$$

and

$$q(r)\in C^1(\Omega) \tag{49}$$

With the proper evaluation of the integral constants, the limits of $g(r)$, $q(r)$ and other relative terms are listed as follows:

$$\lim_{r\to 0}g(r)=-\frac{1}{c^2} \tag{50}$$

$$\lim_{r\to 0}g'(r)=0 \tag{51}$$

$$\lim_{r\to 0}q(r)=0 \tag{52}$$

$$\lim_{r\to 0}q'(r)=\frac{1}{3c^2} \tag{53}$$

$$\lim_{r\to 0}g''(r)=\lim_{r\to 0}\frac{g'(r)}{r}=\frac{1}{3} \tag{54}$$

$$\lim_{r\to 0}\left(q'(r)-\frac{q(r)}{r}\right)=\lim_{r\to 0}\left(\frac{q'(r)}{r}-\frac{q(r)}{r^2}\right)=0 \tag{55}$$

$$\lim_{r\to 0}\left(\frac{q'(r)}{r^2}-\frac{q(r)}{r^3}\right)=-\frac{1}{5} \tag{56}$$

After the derivation of the particular displacements, the corresponding strains, stresses and tractions can be derived through the following formulations:

$$\tilde{\varepsilon}_{ijk}(r)=\frac{1}{2}(\tilde{u}_{ij,k}(r)+\tilde{u}_{ik,j}(r)) \tag{57}$$

$$\tilde{\sigma}_{ijk}(r)=2G\tilde{\varepsilon}_{ijk}(r)+\frac{2G\nu}{1-2\nu}\tilde{\varepsilon}_{imm}(r)\delta_{jk} \tag{58}$$

$$\tilde{p}_{ij}(r)=\tilde{\sigma}_{ijk}(r)n_k \tag{59}$$

5. Numerical examples

Four examples are given in this section. In the first three examples the material properties are simply evaluated:

$$\text{Density}: \quad \rho=1.14 \tag{60}$$

$$\text{Young's modules}: \quad E=1.0 \tag{61}$$

$$\text{Poisson's rate}: \quad \nu=0.25 \tag{62}$$

In the first two examples, the relative error is defined as follow:

$$e=\frac{1}{|v|_{\max}}\sqrt{\frac{1}{N}\sum_{i=1}^{N}(v_i^{(e)}-v_i^{(n)})^2} \tag{63}$$

in which v stands for the concerned variable and $v^{(e)}$,$v^{(n)}$ are the exact value and numerical value, respectively.

In this application, the density of internal RBF points depends on the size of the surface element and is controlled by several parameters. The basic idea for generating the internal RBF points can be described briefly as follows:

(1) Construct an octree in which two points can be kept some distance away.
(2) Create a ray starting from one boundary node and along the negative direction of the outside normal.
(3) Compute the intersection points with all boundary surfaces, find the nearest one.
(4) Generate several points on the segment between the starting point and its corresponding intersection point.
(5) Put the point generated in the step (4) into the octree which is constructed in the first step. Loop until all the points generated in step (4) are done.
(6) Loop from step (2) to step (5) until all the boundary nodes are done.
(7) Store all the points that remain in the octree.
(8) It should be mentioned that the above procedure should be performed after the boundary meshing.

5.1. Dirichlet problem on a torus

In this example, the essential boundary is imposed on the boundary face of a torus. The torus, whose exterior radius and interior radius are of 10 units and of 3 units, respectively, is centered at the origin. This example is presented to show the accuracy and convergence of the DRBFM with comparison to traditional DRBEM.

The analytical solution is given as:

$$\begin{cases} u_1=x^2+y^3+z^3 \\ u_2=x^3+y^2+z^3 \\ u_3=x^3+y^3+z^2 \end{cases} \tag{64}$$

together with appropriately prescribed boundary conditions corresponding to the above analytical solution. The corresponding body force is

$$\begin{cases} b_1=2.4+2.4y+2.4z \\ b_2=2.4x+2.4+2.4z \\ b_3=2.4x+2.4y+2.4 \end{cases} \tag{65}$$

In both of the DRBFM and the DRBEM analysis, displacements and tractions on the boundary are approximated by linear triangle elements. The comparison on convergence is made for 4 sets of elements. The numbers of elements, source points and RBF interpolation points are listed in Table 1.

Figs. 3 and 4 illustrate 770 elements, 436 source points and 1077 RBF centers in one of the DRBFM analysis.

In this example, the variation scheme

$$c_i=\frac{\ln 3}{D_i} \tag{66}$$

is applied.

The errors of tractions on source points (nodes) are shown in Fig. 5.

It is shown in Fig. 5 that the DRBFM is more accurate than the DRBEM with the same number of elements and the same number of RBF centers. It can also be concluded from Fig. 5 that the DRBFM is less sensitive to the mesh density than the DRBEM and that acceptable results can be obtained using a few elements. For example, the relative error of the traction along x direction from

Table 1
Number of elements, source points and RBF points in the first example.

	1	2	3	4
Elements	520	770	1330	2136
Source points	302	436	733	1153
RBF points	420	1077	1952	2503

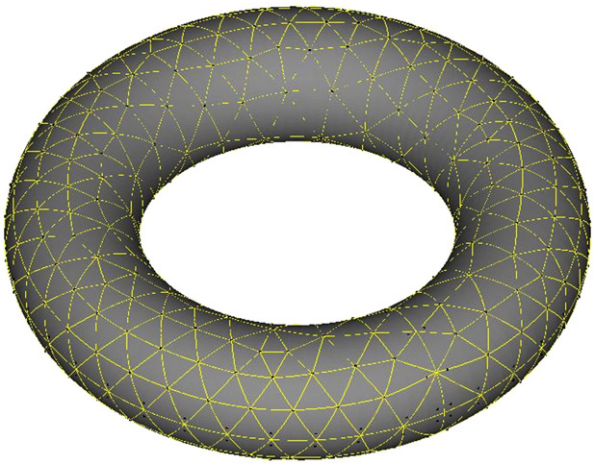

Fig. 3. Discretization of a torus.

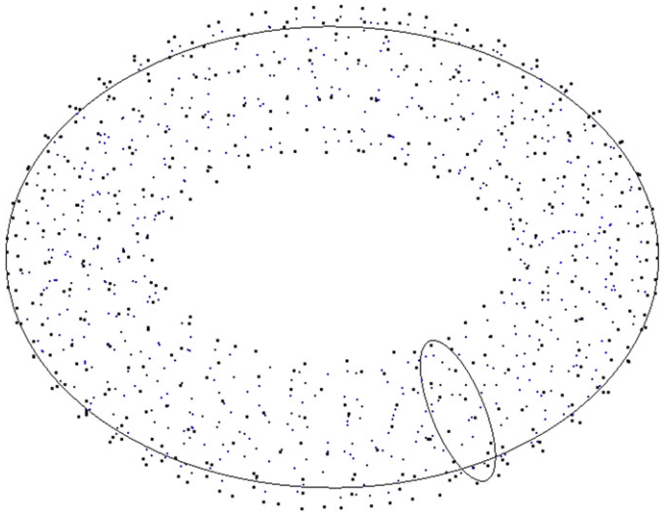

Fig. 4. Distribution of RBF centers.

DRBFM is only 5.14% using 520 elements, and that from DRBEM shoots up to 11.26%. All of these results are reasonable, because in the DRBFM, the geometric data at Gaussian integral points are calculated directly from the faces rather than from elements as in the DRBEM, thus no geometric error is introduced even in a coarse grid.

5.2. Dirichlet problem on a thin cylinder

The second example is presented to show the stability of the VSERBF. We make comparisons between the VSERBF and the constant shaped exponential RBF (CSERBF) on the error of tractions at nodes. The analytical solution, boundary condition and the body force for this problem are the same as those in the first example. The cylinder is of 10 units high, and its outer diameter is

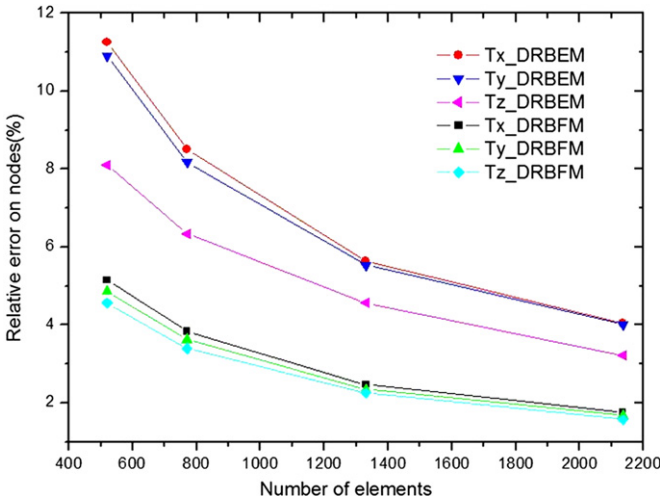

Fig. 5. Comparison on convergence between DRBFM and DRBEM.

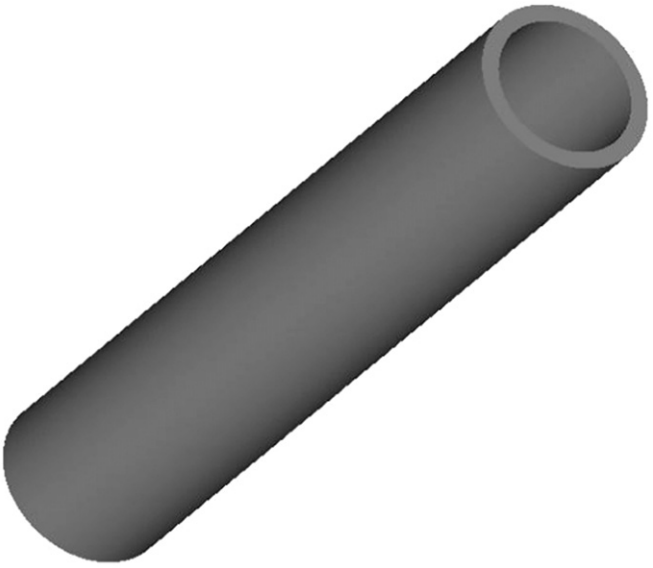

Fig. 6. A cylinder of 0.4 units thick.

of 4 units. Seven cylinders with different thicknesses (0.4, 0.2, 0.1, 0.04, 0.02, 0.01 and 0.008) are considered in this example. Fig. 6 shows a cylinder of 0.4 units thick.

The relative errors of tractions on nodes obtained by two kinds of RBF, the VSERBF and the CSERBF, are illustrated in Fig. 7. The variation scheme Eq. (24) is used to determine the shape parameter of VSERBF with a is taken as ln3. In the case of CSERBF, the constant parameter c in Eq. (22) is taken as 0.1. 474 quadric quadrilateral surface elements and 1634 boundary nodes are used in this computation.

It can be seen from Fig. 7 that the relative errors of tractions on nodes, which are obtained by the constant shaped exponential RBF, becomes unacceptable when the thickness of the cylinder is smaller than 0.02 units. In contrast, the DRBFM equipped with VSERBF is much more stable. A reliable result can be obtained even if the thickness of the cylinder is smaller than 0.01 units. This feature is of great importance for the DRBFM to analyze thin structures.

5.3. Dirichlet problem on an elbow pipe

The third example concerns a pipe structure of elbow shape. The variation scheme for VSERBF we apply in this example is also

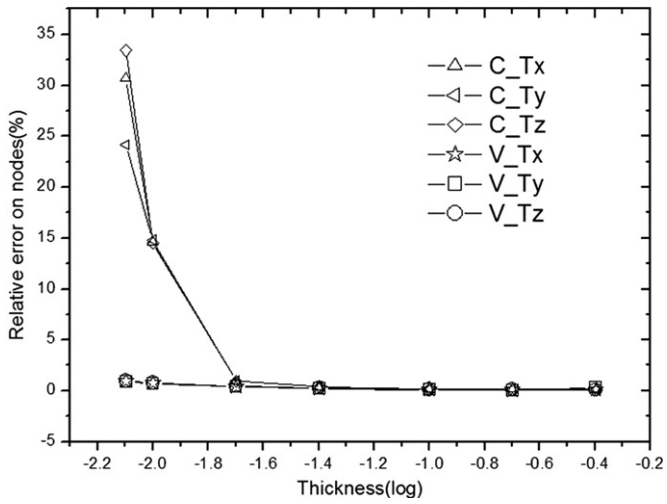

Fig. 7. The accuracy of DRBFM using two kinds of RBF.

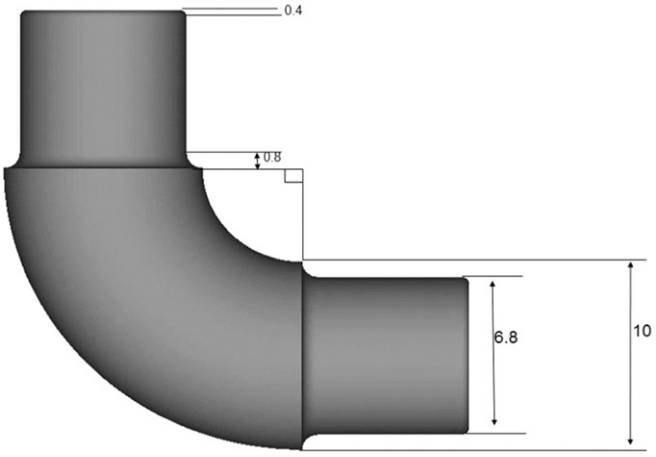

Fig. 8. Illustration of the elbow pipe.

Eq. (66). We compare the numerical two stress results with analytical solution. The size of the elbow pipe is illustrated in Fig. 8, and 50 sample points are distributed uniformly on a circle as shown in Fig. 9. It should be noted that, the sample points are arranged on a circle which is located inside the elbow pipe.

The Dirichlet boundary and the analytical solution for displacement are given by:

$$\begin{cases} u_1 = \cos(0.3x)+\sin(0.3y)+\sin(0.3z) \\ u_2 = \cos(0.3y)+\sin(0.3x)+\sin(0.3z) \\ u_3 = \cos(0.3z)+\sin(0.3y)+\sin(0.3x) \end{cases} \tag{67}$$

The body forces in this example are:

$$\begin{cases} b_1 = -0.108\cos(0.3x)-0.036\sin(0.3y)-0.036\sin(0.3z) \\ b_2 = -0.108\cos(0.3y)-0.036\sin(0.3x)-0.036\sin(0.3z) \\ b_3 = -0.108\cos(0.3z)-0.036\sin(0.3y)-0.036\sin(0.3x) \end{cases} \tag{68}$$

Approximations of physical variables are performed using 448 quadric quadrilateral elements. The comparisons with analytical solution on equivalence stress and on maximal shear stress are shown in Figs. 10 and 11.

It can be concluded from Figs. 10 and 11 that our method is very accurate for the stresses inside the domain even if the analytical solution varies rapidly.

To demonstrate the convergence of the proposed method, we have analyzed this geometric model by a set of quadratic

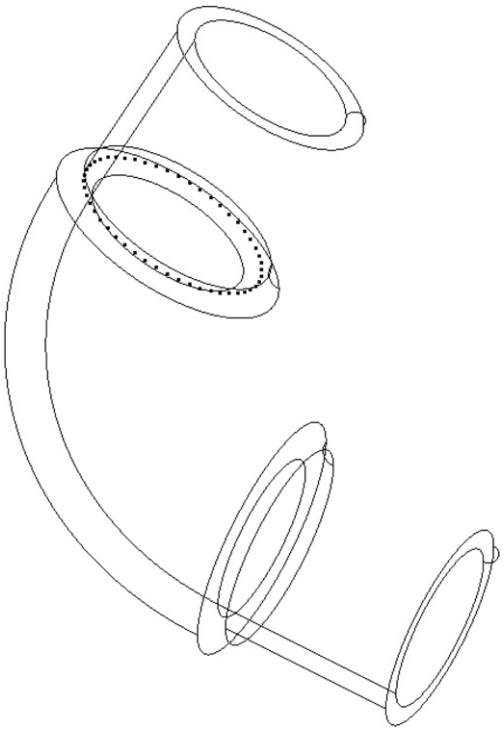

Fig. 9. Location of sample points.

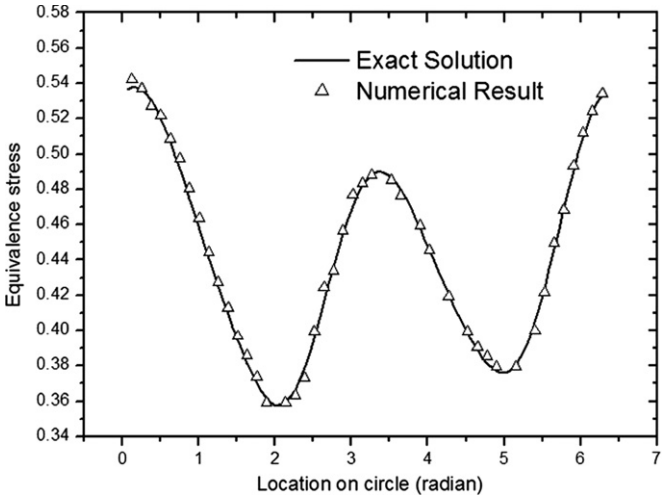

Fig. 10. Comparison on equivalent stress with exact solution.

elements which is listed in Table 2. In this table, NE, NN and NR denote for the number of elements, the number of nodes and the number of radial basis centers, respectively.

The relative errors of the tractions on boundary nodes are calculated and illustrated in Fig. 12.

In Fig. 12, the black line with triangle, the red line with circle and the blue line with square denote the relative error of traction along *X*, *Y* and *Z* direction, respectively. It can be seen from Fig. 12 that the tractions, which are computed by the proposed method, converge to the analytical solution rapidly.

5.4. A cylinder steel pipe with gravity

The last example concerns a practical problem without analytical solution. To validate the accuracy of our method, a comparison study between the DRBFM and the FEM has been made. The

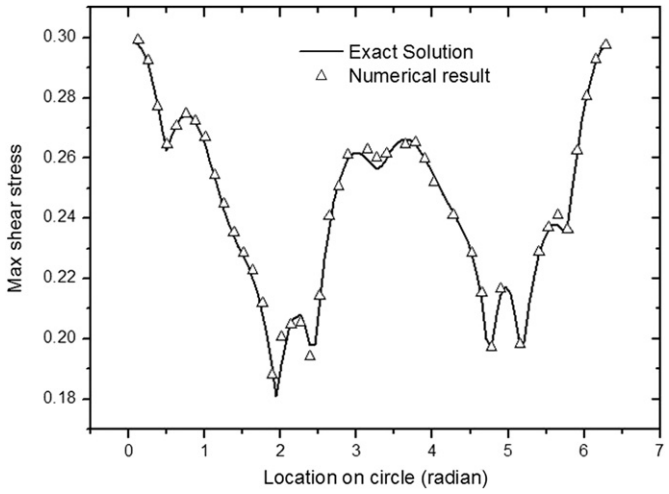

Fig. 11. Comparison on maximal shear stress with exact solution.

Table 2
Number of elements (NE), nodes (NN) and RBF points (NR) in the 3rd example.

	1	2	3	4	5	6	7	8
NE	112	148	176	254	306	368	440	520
NN	482	630	722	996	1186	1378	1618	1890
NR	490	641	736	1005	1387	1464	1954	2225

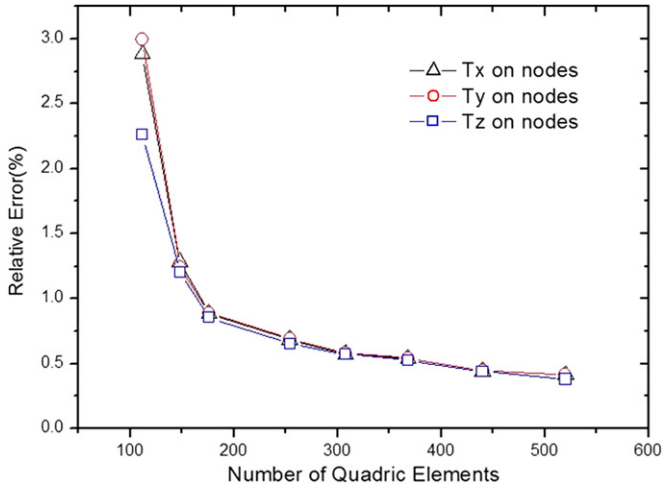

Fig. 12. Convergence study on traction result. (For interpretation of the references to colour in this figure legend, the reader is referred to the web version of this article.)

geometric dimensions of the structure is illustrated Fig. 13. It should be noted that small fillets appear on the structure. These small features are treated without any additional efforts in our method since our method is performed directly on the solid model. In the FEM, however, it is necessary to use a lot of nodes and elements approximate them. Thus the computational scale increases.

The bottom face of the structure is fixed, and a gravity force is applied in the negative direction of the x axis. The Young's module, the density, the Poisson's rate and the gravity acceleration are given as 2.2×10^{11} Pa, 7800 kg/m^3, 0.3 and 9.8 m/s^2, respectively.

In our method, 1461 boundary nodes and 1245 linear parametric Lagrange elements are used. Fig. 14 shows boundary nodes

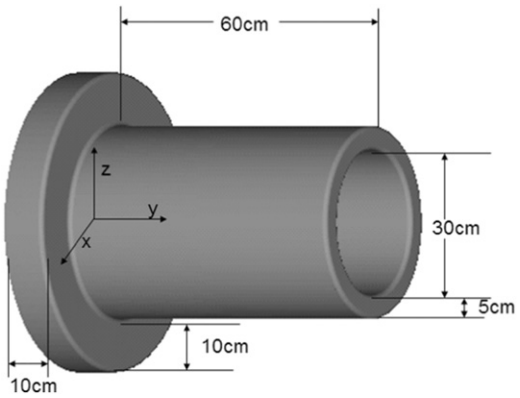

Fig. 13. Illustration of the cylinder pipe.

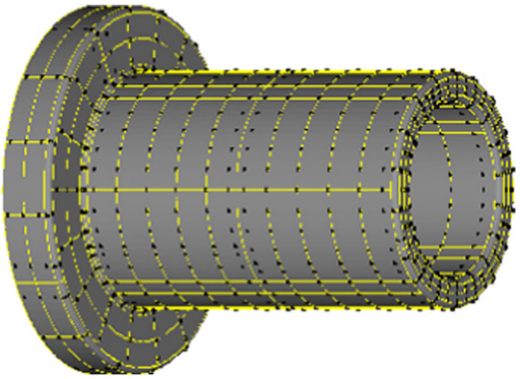

Fig. 14. 1461 boundary nodes and 1245 parametric elements in DRBFM. (For interpretation of the references to colour in this figure legend, the reader is referred to the web version of this article.)

Table 3
The number of nodes and elements used in the FEA.

	1	2	3
Nodes	30,345	40,865	106,145
Elements	6344	8418	22,620

(in black dots) and the boundary elements (in yellow line). Besides the boundary nodes, 2813 points are applied for RBF interpolation. The variation scheme we use in this example is the same as that in the second example.

The finite element analysis (FEA) of this problem was performed by the commercial software ANSYS 12.0. Three FEM implementations are performed with various numbers of nodes and elements as illustrated in Table 3.

The grid model with 8418 quadric elements is illustrated in Fig. 15. We compute the equivalent stress on the blue circle as shown in Fig. 16. It should be pointed out that the place in which the blue circle lies usually concentrates stresses. But it is usually omitted in the FEM for the reasons we introduced before.

Fig. 17 illustrates both results obtained by our method and that by FEM.

In Fig. 17, the equivalent stress distribution obtained by our method is denoted by the black line. Three colored lines denotes for the stress distribution obtained by FEM with 106,145 nodes, 40,865 nodes and 30,545 nodes, respectively. The comparison demonstrates that our method is efficient in calculating stresses. With much less computational costs than that in the FEM, our method can lead to a highly accurate stress result.

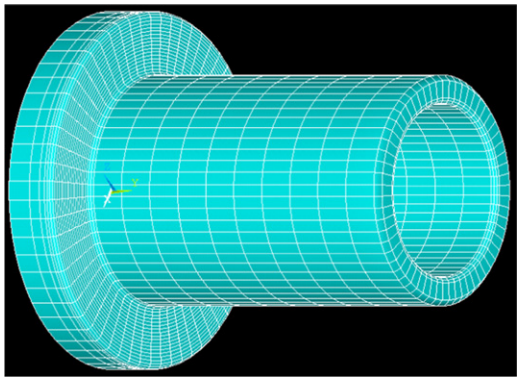

Fig. 15. Grid model with 8418 quadric elements and 40,544 nodes.

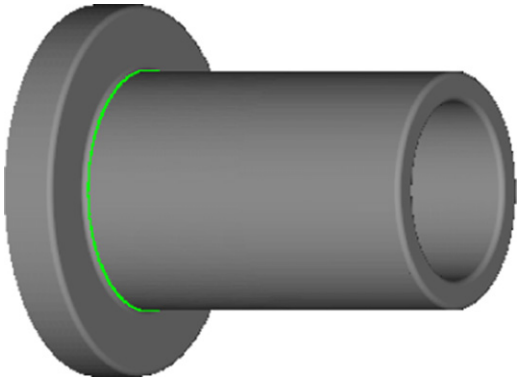

Fig. 16. Locations of the sample points. (For interpretation of the references to colour in this figure legend, the reader is referred to the web version of this article.)

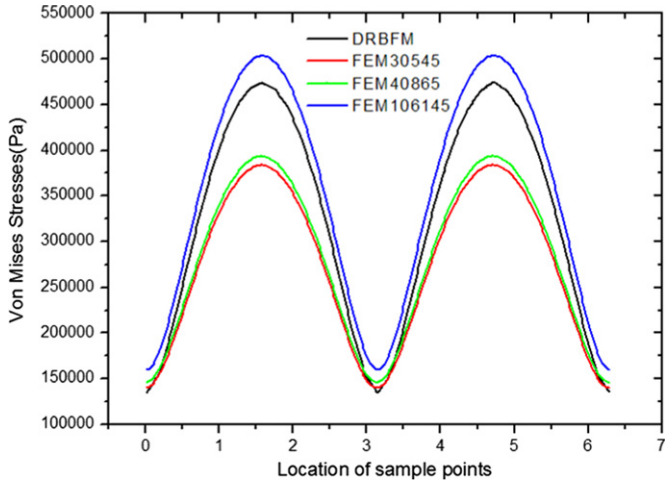

Fig. 17. The equivalent stress on points sampled along the circle. (For interpretation of the references to colour in this figure legend, the reader is referred to the web version of this article.)

It is worth noting that when the pipe becomes thinner, the shell elements should be used in the FEM. The linkage between the shell elements with the Lagrange elements is quite a troublesome task and usually leads to an inaccurate result. In our method, however, the only difficulty for this case is the treatment of the near singular integral [22–25,28–29]. We have also applied our method to analyze a similar steel pipe whose thickness is only 2 cm as shown in Fig. 18. In this application, 1358 nodes, 1181 linear elements and 2028 interpolation points are used. The

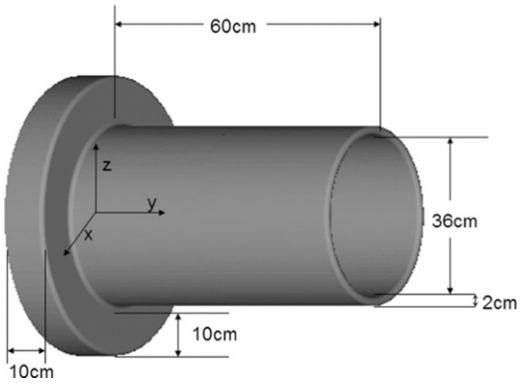

Fig. 18. A thinner steel pipe.

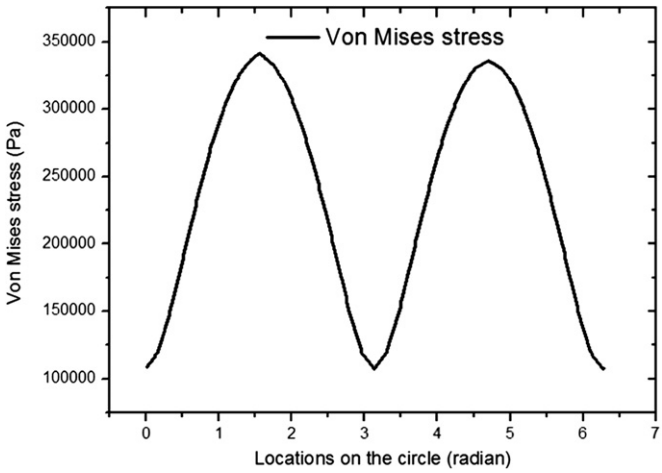

Fig. 19. Equivalent stress on the circle. (For interpretation of the references to colour in this figure legend, the reader is referred to the web version of this article.)

distribution of equivalent stress on the blue circle as mentioned above has been illustrated in Fig. 19. It is sufficient to demonstrate that our method can be applied to solve problems on thin structure with small features efficiently.

6. Conclusions and furture work

The DRM combined with the BFM to solve non-homogeneous elasticity problem is presented in this paper. The DRBFM is implemented based on boundary representation (B-rep) data structure. The geometric data in the quality of the integrals are calculated directly from the boundary faces, thus no geometric error is introduced. This is the main advantage of DRBFM over DRBEM. In the DRBFM, an exponential RBF has been employed. The corresponding particular solution for elasticity has been derived using the method of Popkovich potential. In order to keep stability in analyzing thin structures, we have proposed a variation scheme for the VSERBF.

The DRBFM with the VSERBF has been verified by several numerical examples on different geometries. It has been observed that the solution is accurate for the displacements and stresses on the boundary and inside the domain. The DRBFM can provide much more accurate result than the DRBEM. For the extreme case of problems on thin shell structures, accurate and stable results can be obtained. The implementation of the proposed method has been performed directly on solid models. Thus the thin structures

with small features, which are difficult to analyze by the FEM, can be analyzed without any simplification and assumption.

The DRBFM requires the parametric representation of the surface of a body and locations of some inner interpolation points. In most CAD packages, solids are usually of B-rep. Therefore, the DRBFM has real potential to seamless interact with CAD software. Coupling the DRBFM with CAD software to handle arbitrary surfaces is an ongoing work.

By coupling with the fast multipole method (FMM) [30–35], the DRBFM may be applied to perform large-scale computations for complicated structures. This is also ongoing.

Acknowledgements

This work was supported in part by National Science Foundation of China under grant numbers 10972074 and 11172098, in part by national project under grant number 2011ZX04003-011, and in part by National 973 Project of China under grant number 2010CB328005.

References

[1] Brebbia CA, The Boundary Element Method for Engineers, London Pentech Press, 1978.
[2] Dong CY. Effective elastic properties of doubly periodic array of inclusions of various shapes by the boundary element method. Int J Solids Struct 2006;44:7919–39.
[3] Shen L, Liu YJ. An adaptive fast multipole boundary element method for three-dimensional acoustic wave problems based on the Burton–Miller formulation. Comput Mech 2007;40:461–72.
[4] Yang K, Gao XW. Radial integration BEM for transient heat conduction problems. Eng Anal Boundary Elem 2010;34:557–63.
[5] Zhang JM, Qin XY, Han X, Li. GY. A boundary face method for potential problems in three dimensions. Int J Numer Methods Eng 2008;80:320–37.
[6] Hughes TJR, Cottrell JA, Bazilevs Y. Isogeometric analysis: CAD, finite elements, NURBS, exact geometry and mesh refinement. Comput Meth Appl Mech Eng 2005;194:4135–95.
[7] Cottrell JA, Hughes TJR, Reali A. Studies of refinement and continuity in isogeometric structural analysis. Comput Meth Appl Mech Eng 2007;196:4160–83.
[8] Lipton S, Evans JA, Bazilevs Y, Elguedj T, Hughes TJR. Robustness of isogeometric structural discretizations under severe mesh distortion. Comput Meth Appl Mech Eng 2010;199:357–73.
[9] Zhang JM, Yao ZH. Meshless regular hybrid boundary node method. Comput Model Eng Sci 2001;2:307–18.
[10] Zhang JM, Yao ZH, Li H. A hybrid boundary node method. Int J Numer Methods Eng 2002;53:751–63.
[11] Zhang JM, Yao ZH, Tanaka M. The meshless regular hybrid boundary node method for 2-D linear elasticity. Eng Anal Boundary Elem 2003;27:259–68.
[12] Mukherjee YX, Mukherjee S. The boundary node method for potential problems. Int J Numer Methods Eng 1997;40:797–815.
[13] Chati MK, Mukherjee S. The boundary node method for three-dimensional problems in potential theory. Int J Numer Methods Eng 2000;47:1523–47.
[14] Qin XY, Zhang JM, Li GY, Sheng XM, Song Q. A finite element implementation of the boundary face method for potential problems in three dimensions. Eng Anal Boundary Elem 2010;34:934–43.
[15] Gao XW. The radial integration method for evaluation of domain integrals with boundary-only discretization. Eng Anal Boundary Elem 2002;26:905–16.
[16] Nardini D, Brebbia CA. A New Approach to Free Vibration Analysis Using Boundary Elements, in Boundary Element Methods in Engineering. Southampton and Springer-Verlag, Berlin and New York: Computational Mechanics Publications; 1982.
[17] Kansa EJ, Hon YC. Circumventing the ill-conditioning problem with multiquadric radial basis functions: applications to elliptic partial differential equations. Comput Math Appl 2000;39:123–37.
[18] Sarra SA, Sturgill D. A random variable shape parameter strategy for radial basis function approximation methods. Eng Anal Boundary Elem 2009;33:1239–45.
[19] Li X, Zhu J, Zhang S. A hybrid radial boundary node method based on radial basis point interpolation. Eng Anal Boundary Elem 2009;33:1273–83.
[20] Zhou FL, Zhang JM, Sheng XM, Li GY. Shape variable radial basis function and its application in dual reciprocity boundary face method. Eng Anal Boundary Elem 2011;35:244–52.
[21] Agnantiaris JP, Polyzos D, Beskos DE. Three-dimensional structural vibration analysis by the dual reciprocity BEM. Comput Mech 1998;21:372–81.
[22] Liu YJ. Analysis of shell-like structures by the boundary element method based on 3-D elasticity: formulation and verification. Int J Numer Methods Eng 1998;41:541–58.
[23] Luo JF, Liu YJ, Berger EJ. Analysis of two-dimensional thin structures (from micro- to nano-scales) using the boundary element method. Comput Mech 1998;22:404–12.
[24] Qin QH. Nonlinear analysis of Reissner plates on an elastic foundation by the BEM. Int J Solids Struct 1993;30:3101–11.
[25] Qin QH, Lu M. BEM for crack-inclusion problems of plane thermopiezoelectric solids. Int J Numer Methods Eng 2000;48:1071–88.
[26] Partridge PW, Brebbia CA, Wrobel LC. The Dual Reciprocity Boundary Element Method. Southampton and Springer-Verlag, Berlin and New York: Computational Mechanics Publications; 1992.
[27] Liu YJ, Rudolphi TJ. Some identities for fundamental solutions and their applications to weakly-singular boundary element formulations. Eng Anal Boundary Elem 1991;8:301–11.
[28] Xie GZ, Zhang JM, Qin XY, Li GY. New variable transformations for evaluating nearly singular integrals in 2D boundary element method. Eng Anal Boundary Elem 2011;35:811–7.
[29] Chen XL, Liu YJ. An advanced 3-D boundary element method for characterizations of composite materials. Eng Anal Boundary Elem 2005;29:513–23.
[30] Zhang JM, Tanaka M, Endo M. The hybrid boundary node method accelerated by fast multipole method for 3D potential problems. Int J Numer Methods Eng 2005;63:660–80.
[31] Zhang JM, Tanaka M. Fast HdBNM for large-scale thermal analysis of CNT-reinforced composites. Comput Mech 2008;41:777–87.
[32] Zhang JM, Tanaka M. Adaptive spatial decomposition in fast multipole method. J Comput Phys 2007;226:17–28.
[33] Liu YJ. A new fast multipole boundary element method for solving large-scale two-dimensional elastostatic problems. Int J Numer Methods Eng 2006;65:863–81.
[34] Liu YJ. A fast multipole boundary element method for 2-D multi-domain elastostatic problems based on a dual BIE formulation. Comput Mech 2008;42:761–73.
[35] Liu YJ. Fast Multipole Boundary Element Method—Theory and Applications in Engineering. Cambridge: Cambridge University Press; 2009.